INTERNATIONAL ATOMIC ENERGY AGENCY
UNITED NATIONS EDUCATIONAL, SCIENTIFIC AND CULTURAL ORGANIZATION
INTERNATIONAL CENTRE FOR THEORETICAL PHYSICS
I.C.T.P., P.O. BOX 586, 34100 TRIESTE, ITALY. CABLE: CENTRATOM TRIESTE

SMR/382- 39

WORKSHOP ON SPACE PHYSICS:
"Materials in Micorgravity"
27 February - 17 March 1989

---

# "Analysis of the Low Gravity Tolerance of Bridgman-Stockbarger Crystal Growth I: Steady and Impluse Accelerations"

F. ROSENBERGER
Centre for Microgravity Research
Huntsville, Alabama
USA

---

Submitted to
J. Crystal Growth
February, 1989

# Analysis of the low gravity tolerance of Bridgman-Stockbarger crystal growth. I: Steady and impulse accelerations.

J. Iwan D. Alexander, Jalil Ouazzani
and Franz Rosenberger

Center for Microgravity and Materials Research
University of Alabama in Huntsville
Huntsville, Alabama 35899

**Abstract**

The effects of steady and impulse-type residual accelerations on dopant distributions during directional solidification in 2-D and 3-D "generic" models of the Bridgman-Stockbarger technique have been investigated using numerical models. The calculations are based on the thermo-physical properties of molten germanium doped with a low concentration of gallium. A novel Chebyshev-collocation pseudo-spectral method was used for the solution of the governing momentum-, mass-, and heat-transfer equations. Only convection caused by temperature gradients was considered.

It was found that lateral non-uniformity in composition is very sensitive to the orientation of the steady component of the residual gravity vector and on the particular operating conditions under consideration. For growth rates of several microns per second a steady background level of $10^{-6}$ times that of normal gravity can be tolerated provided that the acceleration vector is aligned with the axis of the growth ampoule. For reduced growth rates, higher (steady) background acceleration levels are acceptable. It was also found that laterally or radially averaged composition profiles are alone insufficient to describe the extent of residual convection in a spacecraft environment. The effects of impulse-type disturbances can be severe and can extend for times on the order of one thousand seconds after the termination of the impulse. A so-called "compensating double pulse" will not result in completely offsetting effects.

## 1. Introduction

During the past decade there has been considerable interest in the possibility of using the almost weightless environment of an orbiting spacecraft as a laboratory in which to study crystal growth processes. The attraction of such a laboratory is that buoyancy-driven convection in nutrient phases may be reduced or practically eliminated so that mass transfer is more likely to be controlled by diffusion [1-3]. It has been recognized for some time that convection can lead to undesirable compositional variations in melt grown (semi-conductor) crystals [2, 4-6]. In many of these cases the convection is buoyancy-driven [7]. Thus, as far as crystal growth is concerned, the diffusion-controlled conditions which may result in a spacecraft should favor compositional uniformity in the crystal [1, 2].

That the magnitude of the effective gravity vector may be reduced as much as six orders of magnitude is well known, and has led to the use of the term *microgravity* to describe the spacecraft's residual acceleration environment. However, our experience in space laboratories has led to the realization that, while in principle the accelerations could be as low as $10^{-5}$ - $10^{-6}$ gal[1], in practice this is not always the case [8,9]. The many sources of residual acceleration [8-10] include the earth's gravity gradient, atmospheric drag, basic orbital attitude motions, crew motions, machinery induced perturbations, and attitude corrections. The latter three can give rise to disturbances on the order of $10^{-3}$ to $10^{-2}$ gal. While these accelerations may be orders

[1] 1 gal = 9.8 m $s^{-2}$, and is a unit of acceleration (named after Galileo) commonly used in geophysics.



of magnitude lower than that experienced at the earth's surface, they are nonetheless finite and pose potential problems for certain types of experiment, especially those for which minimization of accelerations is desirable.

In this work, we examine the extent to which buoyancy-driven convection, caused by small accelerations characteristic of the steady component of the residual acceleration vector in a spacecraft, result in non-uniform solute distribution in a directionally solidified crystal. The physical system under consideration involves crystals grown from a two component melt via the Bridgman-Stockbarger technique. In particular, the importance of ampoule orientation relative to the gravity vector is studied. The effects of impulses are also examined. The consequences of other types of time-dependent disturbances will be discussed in a companion paper.

In previous work involving the use of numerical models to study melt convection, the thermal boundary conditions have been modelled with varying degrees of fidelity. Early work [11-13] includes a variety of imposed temperature boundary conditions. These range from purely vertical temperature gradients in which the flow ensues after a critical value of the Rayleigh number is exceeded [14], to idealized conditions associated with Bridgman-Stockbarger furnaces [13] which are imposed directly on the melt and crystal without consideration of the heat transfer between the ampoule, furnace and sample. For these boundary conditions, flow always occurs owing to the presence of radial temperature gradients. Later models [15,16] have accounted for the presence of the ampoule, and the furnace design. In an actual growth situation the characteristic thermal profile of the inner surface

of the furnace is not realized at the ampoule wall; it is modified by heat transfer between the crystal, melt, ampoule and the furnace itself. The tendency is to reduce axial temperature gradients, while radial temperature gradients may increase or decrease depending on the specific nature of the heat transfer between the charge and ampoule [15]. The influence of melt convection on dopant distribution has been examined for dilute and non-dilute melts [13,15]. For a given furnace-ampoule combination the amount of compositional non-uniformity (or radial segregation) was shown to be a non-linear function of the Rayleigh number. The growth rate and physical properties of the melt also influence the degree of compositional uniformity in the grown crystal.

That residual accelerations on the order of $10^{-6}$ - $10^{-5}$ gal are sufficient to cause observable fluid motion has been established [10,17-19] and can be inferred from work such as [13]. The sensitivity to low gravity has also been estimated for a wide variety of experiments by dimensional analysis [20,21]. The extent to which gravity causes solute redistribution, via buoyancy-driven fluid motion, during directional solidification in geometries characteristic of the Bridgman-Stockbarger technique has been examined using numerical models [11-14,19, 22]. Apart from McFadden and Coriell [22] who examined a two-dimensional situation in which the gravity vector continuously rotates relative to the container, and Polezhaev et al. [19], other work is restricted to axisymmetric situations in which a steady gravity vector is oriented parallel to the axis of a cylindrical ampoule.

A general conclusion that can be drawn from all previous attempts to characterize gravity-driven convective effects on directional



solidification from two components melts (and from the results of the work presented here) is that the maximum lateral solute non-uniformity (radial segregation for the axisymmetric cases) occurs near the transition from diffusion dominated to convection dominated growth conditions [20,23]; that is, when convective velocities are of the same order of magnitude as the diffusive velocities. The conditions under which this "transition" takes place will depend on the specific nature of the forces driving convection. We demonstrate in this work that the orientation of the steady component of the gravity vector is crucial in determining the magnitude of the gravity vector at which this transition occurs. Thus, for a given set of operating conditions the orientation of the gravity vector can determine the suitability of a low gravity environment for directional solidification experiments.

In the following sections we formulate the basic model, define the range of operating conditions under consideration and examine the effects of magnitude and orientation of steady and impulse-type acceleration vectors on compositional uniformity in directionally solidifying crystals. The objective of this work is to identify trends. Rather than attempt to model the thermal conditions corresponding to a specific furnace, we adopt a generic model which is based on the pioneering work of Chang and Brown [13], in which the thermal profile is imposed on the melt and crystal.

**2. Formulation**

The following physical situation, which corresponds to directional solidification by the Bridgman-Stockbarger technique, is considered. An ampoule containing a (dilute) two component melt is translated at a constant rate between fixed hot and cold zones of a furnace. The upper and lower parts of the furnace are maintained at a uniform temperature by means of heat pipes and the two zones are separated by a thermal barrier [24]. Directional solidification takes place as the ampoule is translated. In an actual growth situation the heat transfer conditions between the crystal, melt and ampoule can result in a non-planar crystal-melt interface (for a summary see [24]). Curvature of the solid-liquid interface can result in significant lateral compositional non-uniformity [25,26]. Since we wish to focus attention on the influence of convection on the composition of the crystal we choose to constrain the interface to be planar.

Two- and three-dimensional models are considered. For the 2-D model the dilute binary melt is assumed to occupy a rectangular region $\Omega$ of height L and width W, which is bounded by planar surfaces (see Fig. 1). In the 3-D model the rectangular region is replaced by a circular cylinder with radius W/2.

Translation of the ampoule is modelled by supplying a doped melt of dilute bulk composition $c_\infty$ at a constant velocity $V_M$ at the top of the computational space, and withdrawing a solid of composition $c_s$ (which, in general, will be a function of both space and time) from the bottom. The crystal-melt interface is located at a fixed distance L from the top of the computational space. Thus, the assumption that the ampoule translation rate and the growth rate are equal is implicit.



The thermal barrier which separates the zones is modelled using adiabatic sidewalls of length L/4 (see Fig. 1). The temperature at the interface is taken to be $T_M$, the melting temperature of the crystal, while the upper boundary is held at a higher temperature $T_H$. In an actual experiment, owing to the finite length of the ampoule there is a gradual decrease in length of the melt zone during growth. In this model transient effects related to this change are ignored. Thus, it is assumed that the ampoule is sufficiently long for steady state temperature, concentration and growth rate to be established. The appropriate boundary condition to adopt in this case is the pseudo-steady state condition used by Chang and Brown [13]. The only transient effects to be considered will arise directly from the time-dependent nature of the residual gravity field. We also assume that the contribution of the solute (dopant) to convection is negligible. Free convection is driven by thermal gradients only.

The governing equations are cast in dimensionless form using L, $\kappa/L$ (where $\kappa$ is the melt's thermal diffusivity), $\rho_M\kappa^2/L^2$ (where $\rho_M$ is the melt's density), $T_H$-$T_M$, and $c_\infty$ to scale the lengths, velocity, pressure, temperature and solute concentration, respectively. The dimensionless equations governing momentum, heat and solute transfer in the melt are then

$$\frac{\partial \mathbf{u}}{\partial t} + (\text{grad}\ \mathbf{u})\mathbf{u} = -\text{grad}p + Pr\Delta\mathbf{u} + RaPr\theta g(t), \qquad (1)$$

$$\text{div}\ \mathbf{u} = 0, \qquad (2)$$

$$\frac{\partial \theta}{\partial t} + \mathbf{u} \cdot \mathrm{grad}\,\theta = \Delta \theta, \tag{3}$$

$$\frac{Sc}{Pr}\left(\frac{\partial C}{\partial t} + \mathbf{u} \cdot \mathrm{grad}\, C\right) = \Delta C, \tag{4}$$

where, $\mathbf{u}(\mathbf{x},t)$, $\theta = (T(\mathbf{x},t) - T_M)/(T_H - T_M)$ and C, respectively represent the velocity, temperature and solute concentration. The parameters $Pr=\nu/\kappa$, $Ra= g\beta(T_H-T_M)L^3/\kappa\nu$ and $Sc=\nu/D$ are, respectively, the Prandtl, Rayleigh and Schmidt numbers. The term $\mathbf{g}(t)$ in equation (1) represents the steady or time-dependent gravity vector. The value of g in Ra is taken to be 1 gal, i.e. equal to the gravitational acceleration at the earth's surface. Thus, the magnitude of $\mathbf{g}$ represents the ratio between the actual residual acceleration and g. Table 1 lists the forms of $\mathbf{g}(t)$ used in these calculations.

The following boundary conditions are applied at the crystal-melt interface

$$\theta = 0, \tag{5}$$

$$\mathbf{u}\cdot\mathbf{N} = Pe/\sigma, \tag{6}$$

$$\mathbf{N} \times \mathbf{u} \times \mathbf{N} = \mathbf{0}, \tag{7}$$

$$\frac{\partial C}{\partial z} = \frac{PeSc}{Pr}(1-k)\,C, \tag{8}$$

where $\mathbf{N}$ points into the melt and is the unit vector perpendicular to the planar crystal melt interface, $Pe = V_M L/\kappa$ is the Peclet number, $\sigma = \rho_M/\rho_s$ and k is the distribution coefficient. We define the measure of compositional non-uniformity in the crystal at the interface to be the lateral range in concentration given by



$$\xi = \frac{(c_{smax} - c_{smin})\times 100\%}{c_{av}}.$$

where $c_s$ is the (dimensional) solute concentration in the crystal, and $c_{av}$ is the average concentration. At the "inlet" (z=0) the following boundary conditions are applied

$$\theta = 1, \tag{9}$$

$$\mathbf{u}\cdot\mathbf{N} = Pe\sigma, \tag{10}$$

$$\mathbf{N} \times \mathbf{u} \times \mathbf{N} = \mathbf{0}. \tag{11}$$

$$\frac{\partial C}{\partial z} = \frac{PeSc}{Pr}(C-1), \tag{12}$$

Equations (8) and (12) express conservation of mass at the crystal-melt interface and the inlet respectively. Equations (6) and (10) guarantee continuity of the melt with the crystal and with the supply of melt at the inlet, while equations (7) and (11) ensure no-slip tangent to the interface and the top surface. At the side walls the following conditions are applied

$$\mathrm{grad}\, C \cdot \mathbf{e}_w = 0, \qquad \mathbf{u}\cdot\mathbf{N} = Pe\sigma, \qquad \mathbf{e}_w \cdot \mathbf{u} = 0, \tag{13}$$

along with

$$\theta = 1, \tag{14}$$

in the isothermal zone and

$$\mathrm{grad}\,\theta \cdot \mathbf{e}_w = 0, \tag{15}$$

in the adiabatic zone. Here $\mathbf{e}_w$ is the normal to the ampoule wall.

While the above model will rarely apply to a specific furnace (since details of the heat transfer at the ampoule walls, and between ampoule and furnace are neglected), it nonetheless serves as a reasonable "generic" model with which to carry out a preliminary analysis of a

directional solidification experiment under conditions characteristic of the low gravity environment of space.

For the most part, our calculations are limited to thermo-physical properties corresponding to dilute gallium-doped germanium, although the effect of different Schmidt numbers are considered for a limited range of steady low gravity conditions. The values of the thermo-physical properties and the associated dimensionless groups and operating conditions are given in Table 2.

### 3. Method of solution

The governing equations (1)-(15) were solved by two different methods; a pseudo-spectral Chebyshev collocation method and a finite volume method implemented by the code PHOENICS [28]. The latter method was used to obtain most of the results pertaining to the Ge:Ga system. PHOENICS was used to obtain two and three dimensional results for Sc = 10. The pseudo-spectral method was found to cope better with the steep solute gradients which occur in the high Schmidt number cases.

The pseudo-spectral method employed is an orthogonal collocation pseudo-spectral method which uses Chebyshev polynomial expansions for spatial discretization [27,29]. Only the two-dimensional calculations were tackled using this approach, although the method is readily extended to three dimensions. Steady solutions are obtained using a pseudo-unsteady method which involves a generalized ADI procedure [27]. The momentum equations are linked to the continuity equation via the method of artificial compressibility. Both steady and time-dependent solutions were computed using an



Adams-Bashforth-Crank-Nicolson scheme [27]. (For more details see [30].) The results presented in this paper were computed using 33×33 points. This was found to yield sufficient resolution for the range of Schmidt numbers considered. For the impulse-type residual accelerations a variable time step was employed. In order to assess the consequences of adopting the pseudo-steady state conditions, (9-12), we varied the aspect ratio of the computational space. While, for accelerations between $10^{-4}$ -$10^{-3}$ gal (oriented parallel to the interface) this altered the flow pattern in the upper part of the ampoule, the computed values of $\xi$ differed only by a few percent from the values computed with aspect ratio 1. For the lower acceleration magnitudes (and for orientations perpendicular to the interface) no significant difference in $\xi$ was found.

PHOENICS embodies a finite volume or finite domain formulation [28,31]. It represents the governing equations introduced in the previous section as a set of algebraic equations. These equations represent the consequence of integrating the differential equation over the finite volume of a computational cell (and, for transient problems, over a finite time) and approximating the resulting volume, area and time averages by interpolation. For the 2-D and axisymmetric calculations discussed in this paper we employed a 40x39 grid. The 3-D calculations were performed in a circular cylindrical domain with 20 nodes in the radial direction, 12 in the azimuthal direction and 39 in the axial direction. We found that for the 2-D calculation less than 40 points in the direction parallel to the interface resulted in poor convergence of the solute field.

The scheme employed by PHOENICS has the same accuracy as a finite difference scheme which is of the order $\Delta x$, where $\Delta x$ is the distance between the grid nodes. The time scheme is implicit and thus unconditionally stable. However, small time steps are required to obtain accurate solutions. For highly non-linear flows the use of under-relaxation is necessary to eliminate divergence and to ensure good convergence of the solutions.

Steady calculations using the pseudo-spectral method with 33x33 collocation points required 2000-2500 iterations to achieve good convergence for the steady calculations. This typically took around 5-10 minutes of (CRAY XMP) CPU time. The finite volume calculations were carried out on a VAX-785 and required 3-4 hours of CPU time.

## 4. Results

### 4.1 Steady accelerations: 2-D

The temperature field is insensitive to the convective motion owing to the low Prandtl number of the melt ($Pr = 10^{-2}$) and the low magnitude of the residual accelerations considered. It is characterized by the conduction profile shown in Fig. 2. Note that there are lateral (radial) as well as axial temperature gradients in the system. The consequent density gradient is responsible, as we shall see, for driving convection in the melt even when residual acceleration magnitudes are as low as $10^{-6}$ gal. The temperature fields for all the cases listed in table 2 are qualitatively similar, the major differences are the magnitudes of the temperature gradients which reflect the temperature difference $T_H - T_M$.



The velocity and concentration distributions, together with the interfacial $\xi$ values, have been obtained for various combinations of orientations and magnitudes of the acceleration vector, growth rates, ampoule ($\Omega$) dimensions and temperature differences $T_H - T_M$. The results are summarized in table 3.

Figs. 3-5 illustrate the velocity and solute fields for three cases where the residual acceleration is parallel to the crystal-melt interface and the operating conditions correspond to **A - V1** in table 2. Note that the vectors in these figures are scaled by the growth velocity and have been obtained by interpolation from the computed values obtained on the unevenly spaced Chebyshev mesh. If the conditions were purely diffusive the velocity vectors would all be the same length and perpendicular to the crystal-melt interface. Furthermore, the isoconcentrates and crystal-melt interface would be parallel. A single roll is calculated at $10^{-5}$ gal, resulting in $\xi = 92.7\%$. Between $10^{-5}$ gal and $10^{-6}$ gal the roll is no longer present and at $10^{-6}$ gal the convective motion results in a barely perceptible deflection of the velocity vectors from a purely longitudinal flow. The compositional variations in the melt are, however, still significant even at $10^{-6}$ gal.

In contrast to the single roll flow depicted in Fig. 3a, Fig. 6 shows that when the same magnitude gravity vector is oriented perpendicular to the crystal-melt interface there are no rolls. The flow is deflected symmetrically about the ampoule axis. The associated compositional non-uniformity is symmetric about the centerline of the ampoule and, with $\xi = 6.4\%$, is significantly smaller than for the asymmetric case.

Fig. 7a-c depicts the lateral variation in composition of the crystal for gravity orientations parallel, at 45° and perpendicular to the interface. These figures further illustrate the importance of ampoule orientation with respect to the residual acceleration vector. For a fixed acceleration magnitude, as the ampoule axis and acceleration vector are brought into alignment, the transition from asymmetric to symmetric compositional non-uniformity is accompanied by a reduction in the magnitude of the non-uniformity. For these, and other cases corresponding to gallium-doped germanium crystals, the values of lateral non-uniformity $\xi$ are listed in table 3 along with the associated operating conditions.

Characterization of melt grown crystals often includes radially or laterally averaged crystal composition profiles [32-34]. Laterally averaged *melt* composition profiles are shown in Fig. 8 for operating conditions corresponding to **A - V1** in table 2 and for a selection of residual accelerations. Note that in Fig. 8b these profiles are indistinguishable from the pure diffusion case. In addition, these profiles, reveal a the high concentration gradient region adjacent to the interface with an approximate width of 0.2 cm. This agrees well with the simple characteristic length obtained from the relation $\delta = D/V_M$.

The consequences of reducing the growth rate are illustrated by Fig. 9 which was obtained for $10^{-5}$ gal parallel to the interface and operating condtions **A - V3** (i.e. $V_M = 0.65\mu m\ s^{-1}$). A comparison of Figs. 3a and 9a shows that due to the reduced melt translation rate the buoyancy-driven recirculation now dominates. Thus, the axial concentration gradient is reduced (Figs. 3b and 9b) and a smaller



concentration gradient along the interface results (in Fig. 9b $\xi$ = 11.9% as compared to 92.7% in Fig. 3b).

Table 3 also illustrates the effect of changing the temperature gradient and the ampoule dimensions. For an acceleration of $10^{-5}$ gal oriented parallel to the interface a reduction of the temperature difference between the hot zone and the crystal-melt interface from 100 K to 20 K changes $\xi$ from 92.7% to 22.6%. An increase in the width of the ampoule from 1 to 2 cm with the 20 K temperature difference yields $\xi$ = 64.5%. Clearly, for a given steady acceleration the value of $\xi$ is sensitive to the particular operating conditions employed.

In order to ascertain the importance of the diffusivity of the dopant we have also examined cases with Sc = 10, 20, 30, and 50 for operating conditions otherwise corresponding to **A - V1**. (Recall that in the relative weighting of convective and diffusive fluxes, an increase in Sc corresponds to a reduction in diffusive transport.) The results are displayed in Fig 10. It is clear that, all other things being equal, the relationship between Sc and $\xi$ is not linear. In particular, for acceleration magnitudes of $10^{-6}$ gal and $10^{-5}$ gal oriented parallel to the interface, the maximum value of $\xi$ is attained for Sc = 20, while at $10^{-5}$ gal oriented perpendicular to the interface there is little difference in the degree of non-uniformity between Sc=20 and 50. Laterally averaged composition profiles for $10^{-4}$ gal acting parallel to the interface are depicted for Sc = 10, 20, 30, and 50 in Fig. 11. In comparison to Fig. 8 the laterally averaged composition profiles at $10^{-4}$ gal exhibit a flat section owing to the increase in convective transport.

**4.2 Steady accelerations: 3-D and axisymmetric**

Five three-dimensional calculations were undertaken for R = 0.5 cm and $V_M$ = 6.5 μm $s^{-1}$ in order to examine the influence of a more realistic geometry. In all cases the operating conditions corresponded to **B - V1** in table 2. Three runs were axisymmetric, with **g** anti-parallel and parallel to **N**. These calculations were carried out (for comparison purposes) with $||\mathbf{g}|| = 10^{-4}$ gal, $10^{-3}$ gal and $10^{-2}$ gal. Values of the radial segregation were found to be within 5% of the values computed for these conditions by Chang and Brown. The compositional non-uniformity ξ was found to be approximately 10% lower for the $10^{-4}$ gal axisymmetric case than for the 2-D analog.

The remaining calculations were fully three-dimensional with **g** parallel to the crystal-melt interface. The fully 3-D cases were carried out for $||\mathbf{g}|| = \sqrt{2}(10)^{-5}$ gal and $\sqrt{2}(10)^{-6}$ gal. The melt isoconcentrates at the interface are shown in Figs. 12 and 13 for sections cut perpendicular to the ampoule axis at z= 1. At the higher value of the residual acceleration, ξ = 91%, which is approximately half the 2-D value. At $\sqrt{2}(10)^{-6}$ gal, ξ = 26%. Thus, for this case, there was little difference between the 2- and 3-D predictions (see table 3).

**4.3 Impulse-type accelerations**

Five cases of impulse-type disturbances were examined. All impulses were superimposed onto a steady background acceleration which was oriented parallel to the crystal-melt interface. The results are summarized in table 4.

Figs. 14(a-d) illustrate the development of the solute field following a one second $5(10^{-3})$ gal impulse oriented anti-parallel to a



background acceleration of $10^{-6}$ gal for operating conditions corresponding to **A - V1**. The effects are long lasting. The velocity field relaxes back to the initial state after some 300 seconds have elapsed. The response of the solute field is slower. The effect of the impulse is to initially re-orient the flow field. This has the effect of first reducing the lateral compositional non-uniformity. Thirty seconds after the termination of the impulse the composition nonuniformity is beginning to increase but has the opposite sense in comparison to the initial non-uniformity (see Figs. 14 a and b). At approximately 260 seconds after the termination of the impulse, ξ reaches a maximum value of 40%. It then slowly decreases in value (Figs. 14 c and d), reverses sense and eventually reaches its initial steady level (Fig. 5 b) after more than 2000 seconds have elapsed.

A shorter duration ($10^{-1}$ second) pulse, with the same orientation and magnitude, resulted in a maximum deviation of the lateral non-uniformity of only 5% from the initial steady level 350 seconds after the termination of the pulse.

The effects of two one-second pulses separated by one second were also calculated. The magnitude of the pulses was $3x10^{-3}$ gal. They were oriented parallel to the crystal interface and superimposed onto a steady background acceleration of $\sqrt{2}x10^{-6}$ gal oriented parallel to the interface. The main effect was to drive ξ from 21.5% (the initial value) to 76% after 225 seconds.

In addition, double pulses were examined. A pulse anti-parallel to the background steady acceleration followed by an equal but opposite pulse does not result in a "null" effect. While the flow generated by the first pulse is reversed by the second pulse there is a net flow following

the termination of the second pulse. This flow is in the same sense as the initial steady flow and results in an increase of the lateral non-uniformity in composition to a maximum of 24% at 100 seconds, whereupon it decays slowly to its initial value.

### 5. Summary and Discussion

The effects on dopant uniformity during directional solidification of steady and impulse-type residual accelerations have been calculated using 2- and 3-dimensional "generic" models of the Bridgman-Stockbarger crystal growth technique. The salient results of our calculations for materials with properties and growth conditions corresponding to those listed in table 2 can be summarized as follows:

For a fixed growth rate, the amount of lateral non-uniformity in composition is very sensitive to the orientation of the steady component of the residual gravity vector. The worst case appears to be when the acceleration vector is parallel to the crystal interface. At growth rates on the order of microns per second, this orientation can lead to non-uniformities of 10-20% when the magnitude of the acceleration is $10^{-6}$ gal. If, however the growth rate is lowered by an order of magnitude, the non-uniformity is reduced significantly. A steady background level on the order of $10^{-6}$ gal can be tolerated for a wide range of the operating conditions examined provided that the acceleration vector is *aligned with the axis of the growth ampoule.*

When **g** is oriented parallel to the crystal-melt interface, the maximum compositional non-uniformity occurs between $10^{-4}$ and $10^{-5}$ gal compared to $10^{-2}$ gal for the axisymmetric case. It is evident upon examination of table 3 and Figs 3-7 that for a given orientation the



relationship between the magnitude of the gravity vector and the amount of compositional non-uniformity is clearly not linear. (This result was first obtained by Chang and Brown [13] for the axisymmetric case).

The effect of a reduction in growth rate on the velocity profile is to shift the center of the convective roll (see Figs. 9a and 3a). This can be explained in terms of the superposition of the uniform solidification flow and a single convective roll. When convective velocities have the same order of magnitude as the solidification velocity the roll center is shifted to one side because only here does the addition of the convective and uniform solidification flow result in no motion.

For the cases examined, a reduction in compositional non-uniformity was also associated with a reduction in $T_H$-$T_M$. The presence of the adiabatic zone results in lateral as well as axial temperature gradients. Thus, convection always occurs in this system since there is always a location where the temperature gradient has a component normal to the acceleration vector. We compared our results with those of Chang and Brown's axisymmetric calculations [13]. Our 3-D axisymmetric computations were found to be in agreement with their work. In addition we carried out full 3-D (*non-axisymmetric*) steady calculations in order to calibrate our 2-D results. For one set of examples we found that with $\sqrt{2}(10)^{-5}$ gal parallel to the interface the percentage compositional non-uniformity predicted by the 2-D calculation ($\xi$ = 152%) was 50% higher than predicted by the full 3-D calculation. This difference may be attributed to the increased surface to volume ratio which increases the effect of the "no-slip" boundary condition. The presence of the rigid walls somewhat retards

the flow and, thus, in comparison to the 2-D case, the degree of solute redistribution is decreased. A comparison between 2- and 3-D calculations for $\sqrt{2}(10)^{-6}$ gal revealed no significant difference in $\xi$. At this magnitude of the gravity vector, convection is localized and weak. The increase in surface to volume ratio for this 3-D case has little influence on the transport conditions.

There are several instances in the literature where radially or laterally averaged *crystal* composition profiles are used to compare space and earth grown samples [32-34]. The space grown samples are usually described as having profiles characteristic of diffusive conditions. A comparison of the laterally averaged melt composition profiles depicted in Figs. 8 and 11 shows that at higher acceleration magnitudes ($10^{-4}$ gal) the flow is able to reduce the concentration gradient way from the interface. This results in the characteristic flat mid-section exhibited by the curves in Fig. 11. This is in contrast to the pure diffusion profile which posses no flat section. However, our calculations show that convection can have significant effects on the lateral variation in composition of both melt and crystal even when the laterally averaged *melt* composition profiles have so-called diffusive profiles. Thus, we propose that radially or laterally averaged composition profiles are alone not sufficient to describe the extent of residual convection during solidification in a spacecraft environment.

The effects of impulse-type disturbances can be severe and can extend for a long time (on the order of $10^3$ seconds) after the termination of the impulse. This is not surprising if one considers characteristic times for momentum and solute diffusion given by $t_m = L^2/\nu$ and $t_s = L^2/D$, respectively. For L = 0.5 cm (corresponding to the



maximum distance from a wall in the 2-D system considered) these characteristic times are $t_m$ ~200 s, and $t_s$ ~ 2000 s, which compare well with the order of magnitude of the decay times given in table 4. A pulse with a one second duration, or a combination of such pulses has a drastic effect on the segregation levels at pulse amplitudes of $10^{-3}$ gal. The nature of the response depends on the magnitude, direction and duration of the impulse, and whether sequential, opposing impulses are involved. A so-called "compensating" double pulse will not result in completely offsetting effects. For the case we examined, however, the resulting compositional non-uniformity was not as severe as for sequential pulses with the same orientation. Further investigation of more realistic impulses (g-jitter) is necessary since the response of the system appears to depend on the nature of the impulse and our results indicate that impulses appear to have important consequences for transient behavior in crystal growth systems.

In addition to the results obtained for Ge:Ga, we have also examined the effects of different physical properties by examining a range of Schmidt numbers. Our results show that, for a given steady acceleration the sensitivity of the process also depends on the operating conditions and the physical properties of the melt. That is, the sensitivity to the residual acceleration depends on temperature boundary conditions, the growth rate, and the ratio of the kinematic viscosity to the solute diffusivity. The fact that in a spacecraft buoyancy forces may be reduced by 5-6 orders of magnitude does not imply that the environment may be considered purely diffusive. Careful evaluation of the interaction between the operating conditions, physical

properties and spacecraft acceleration environment must be made in order to ensure optimum use of limited spaceflight opportunities.

Space flight experiments involving germanium have been carried out on Skylab [32,34] and the Apollo-Soyuz Test Project (ASTP) [35,36]. The latter involved the directional solidification of seeded Ge melts. Melts were doped with gallium and some were doped with 1% Si and .001% Sb [36]. These results have generated some controversy [1]: lateral compositional profiles revealed strong asymmetric non-uniformities in the space grown crystals. Lateral variations were also observed in samples grown under terrestrial conditions but were much less pronounced [1]. In order to explain these observations it has been argued that the asymmetric redistribution of the dopant can be ascribed to "barometric diffusion" of the solutes due to the acceleration gradient in the melt arising from the rotational motion of the spacecraft [35,36]. The basis of the argument, however, appears to ignore the presence of gravity gradient and atmospheric drag effects and does not explicitly account for the spacecraft attitude motions. If it is assumed that during this phase of the ASTP mission the spacecraft flew in a radial attitude [9] (i.e. it continuously rotated relative to a fixed geocentric frame), then a steady residual acceleration vector would result from the gravity gradient, atmospheric drag and centrifugal contributions to the relative acceleration. It has been demonstrated in this work that melt convection can occur in response to a steady residual acceleration of rather small magnitudes. Furthermore, whenever the acceleration vector is not aligned with the ampoule axis strong asymmetries in the solute composition profiles can occur. Since the dependence of



composition uniformity on convection is not linear, and since small asymmetries in temperature profiles can lead to asymmetric convection [37], there is always the possibility that the observed non-uniformities in the terrestrially grown samples will be smaller than those observed in space grown samples. Thus, the probability that the strong asymmetries in composition observed in the space-grown samples can be attributed to residual acceleration effects should not be discounted.

It should be emphasized that while some of the conditions examined have shown great sensitivity to residual acceleration, we have also shown that there are combinations of operating conditions for which the effects of realsitic residual acceleration levels are small. It is therefore clear that residual gravity effects should be seriously considered when planning optimal operating conditions for space experiments. Furthermore, since our results are generic in nature they cannot be substituted for a detailed numerical examination of a particular Bridgman-type crystal growth system, although they can be expected to indicate trends in the expected response to the steady residual acceleration environment. As far as the response to time-dependent accelerations is concerned, impulses have been shown to be important, but more work is needed in this area, especially in terms of a more realistic representation of the residual acceleration vector. Continuous periodic accelerations are also a concern [21], particularly in the low frequency range (~$10^{-3}$ Hz) and will be examined in a companion paper [38].

---

Acknowledgements

This work was supported by the National Aeronautics and Space Administration under grant NAG8-684, by the State of Alabama through the Center for Microgravity and Materials Research at the University of Alabama in Huntsville, and through the Alabama Supercomputer Network. We would like to thank Dr. Robert Naumann for stimulating our interest in this problem.

## References

[1] J. T. Hurle, G. Müller and R. Nitsche, in *Fluid Sciences and Materials Science in Space. A European Perspective.* Ed. H. U. Walter (Springer, Berlin, 1987) p. 315.

[2] F. Rosenberger, *Fundamentals of Crystal Growth I.* Springer Series in Solid-State Sciences, Vol. 5, (Springer, Berlin, 1979).

[3] R. F. Sekerka and S. R. Coriell, *Proc. 3rd European symposium on materials sciences in space*, Grenoble France, April 1979, ESA SP-142 (1979) 55.

[4] S. M. Pimputkar and S. Ostrach, *J. Crystal Growth* **55** (1981) 614.

[5] G. Müller, in *Convective transport and instability phenomena*, Eds. J. Zierep and H. Oertel (Braun, Karlsruhe, 1982) p. 441.

[6] G. Müller, G. Neumann, and W. Weber, *J. Crystal Growth* **70** (1984) 78.

[7] W. E. Langlois, *Ann. Rev. Fluid Mech.* **17** (1985) 191.

[8] H. Hamacher, R. Jilg, U. Mehrbold, *Proc. 6th European symposium on materials sciences under microgravity conditions*, Bordeaux, France Dec 2-5 1986, ESA SP-256 (1987) p. 413.

[9] J. I. D. Alexander and C. A. Lundquist,*J. Astr. Sci.* **35** (1987) 193.

[10] J. I. D. Alexander and C. A. Lundquist, *AIAA Journal* **26** (1988) 193.

[11] P. A. Clark and W. R. Wilcox, *J. Crystal Growth* **50** (1980) 461.

[12] N. Kobayashi and W. R. Wilcox, *J. Crystal Growth* **59** (1982) 616.



[13] C. J. Chang, an R. A. Brown, *J. Crystal Growth* **63** (1983) 353.

[14] G. B. McFadden, R. G. Rehm, S. R. Coriell, W. Clark and K. A. Morrish, *Metall. Trans.* **A15** (1984) 2125.

[15] P. M. Adornato and R. A. Brown, *J. Crystal Growth* **80** (1987) 155.

[16] D. H. Kim, P. M. Adornato and R. A. Brown,*J. Crystal Growth* **89** (1988) 339.

[17] Y. Kamotani, A. Prasad and S. Ostrach, *AIAA Journal* **19** (1981) 511.

[18] V. I. Polezhaev, *Hydrodynamics, heat and mass transfer during crystal growth* in *Crystals* **10** Ed. H. C. Freyhardt (Springer, Berlin, 1984).

[19] V. I. Polezhaev, A. P. Lebedev and S. A. Nikitin, *Proc. 5th European symposium on materials sciences under microgravity*, Schloss Elmau FRG, ESA SP-222 (1984 ), p. 237.

[20] D. Camel, and J. J. Favier, *J. de Physique* **47** (1986) 1001.

[21] R. Monti, J. J. Favier and D. Langbein, in *Fluid sciences and materials science in space, a European perspective.* Ed. H. U. Walter (Springer, Berlin, 1987) p.637.

[22] G. B. McFadden, and S. R. Coriell, in *Proc. AIAA/ASME/SIAM/APS 1st National Fluid Dynamics Congress*, Cincinnati, July 25th-28th (1988) p. 1572.

[23] A. Rouzaud, D. Camel and J. J. Favier, *J. Crystal Growth* **73** (1985) 149.

[24] Y. M. Dakhoul, R. Farmer, S. L. Lehoczky and F. R. Szofran, *J. Crystal Growth* **86** (1988) 49.

[25] S. R. Coriell and R. F. Sekerka, *J. Crystal Growth* **46** (1979) 479.

[26] S. R. Coriell, R. F. Boisvert, R. G. Rehm and R. F. Sekerka, *J. Crystal Growth* **54** (1981) 167.

[27] R. Peyret and T. D. Taylor *Computational Methods for Fluid Flow* (Springer, New York, 1983).

[28] H. I. Rosten and D. B. Spalding, in *Lecture Notes in Engineering* Eds. C. A. Brennia and S. A. Orszag Vol. 18 (Springer, New York, 1986) p. 3.

[29] J. Ouazzani and R. Peyret, *Proc. 5th GAMM Conference on Numerical Methods in Fluid Mechanics*, Rome, 5th-7th October 1983, M. Pandolfi and R. Piva eds. (Vieweg and Sohn, Braunschweig, 1983) 275.

[30] J. Ouazzani, *A new iterative method for unsteady incompressible fluid flows using a collocation pseudo-spectral technique*. To be published...(1989).

[31] S. V. Patankar, *Numerical Heat Transfer and Fluid Flow* (Hemisphere Publishing, Washington, 1980).

[32] J. T. Yue and F. W. Voltmer, *J. Crystal Growth* **29** (1975) 329.

[33] H. C. Gatos Materials Processing in the Reduced Gravity Environment of Space ed. G Rindone (Elsevier, New York, 1982) 355.

[34] A. F. Witt, H. C. Gatos, M. Lichtensteiger, M. C. Lavine and C. J. Herman J. Electrochem Soc. 125 (1975) 276.

[35] V. S. Zemskov, *Soviet Physics Dokl.* **22** (1977) 170.

[36] V. S. Zemskov, I. L. Shul'pina, A. N. Titkov, I. Belokurova, N. B. Guseva, and V. I. Safarov, *Soviet Phys. Solid State* **21** (1979) 576.

[37] St. Krukowski, J. Iwan D. Alexander, J. Ouazzani and F. Rosenberger, *Convection in an asymmetrically heated ampoule*, to be published.

[38] J. I. D. Alexander, J. Ouazzani and F. Rosenberger *Analysis of the low gravity tolerance of Bridgman-Stockbarger crystal growth II: Transient and periodic accelerations*, in preparation 1989.

Table 1. Forms of the acceleration vector examined in this work.

**Steady**

$\mathbf{g}_o = g_{ox}\,\mathbf{i} + g_{oz}\,\mathbf{k}$;

$||\mathbf{g}|| = 10^{-4},\ \sqrt{2}\times10^{-5},\ 10^{-5},\ 5\sqrt{2}\times10^{-6},\ 5\times10^{-6},\ \sqrt{2}\times10^{-6},$

$10^{-6},\ 10^{-7}$

**Impulse**

$\mathbf{g}(t) = [g_o + g(t)]\mathbf{k}$ , $\quad g_o = 10^{-6},\ \sqrt{2}\times10^{-6}$.

$g(t) = 0$ for $t < t_1$ and $t > t_2$ , and $g(t) = g_1$ for $t_1 < t < t_2$ ;

$g(t) = 0$ for $t < t_1$ , $t_2 < t < t_3$ and $t > t_4$ ,
and $g(t) = g_1$ for $t_1 < t < t_2$ , $t_3 < t < t_4$ ;
$g(t) = 0$ for $t < t_1$ , $t_2 < t < t_3$ and $t > t_4$ ,
and $g(t) = g_1$ for $t_1 < t < t_2$ , $g(t) = -g_1$ for $t_3 < t < t_4$ ;
$g_1 = 5\times10^{-3},\ 3\times10^{-3}$.

Table 2 Thermo-physical properties of gallium-doped germanium [13] and operating conditions used in the calcualtions

| | Property | Value |
|---|---|---|
| | Thermal conductivity of the melt | 0.17 $WK^{-1}\,cm^{-1}$ |
| | Heat capacity of the melt | 0.39 $Jg^{-1}K^{-1}$ |
| | Density of the melt ($\rho_M$) | 5.6 g $cm^{-3}$ |
| | Density of the solid ($\rho_S$) | 5.6 g $cm^{-3}$ |
| | Kinematic viscosity of the melt ($\nu$) | 1.3 $(10)^{-3}$ $cm^2s^{-1}$ |
| | Melting temperature ($T_M$) | 1231 K |
| | Solute diffusivity (D) | $1.3(10)^{-4}$ $cm^2s^{-1}$ |
| | Thermal diffusivity of the melt ($\kappa$) | $1.3(10)^{-1}$ $cm^2s^{-1}$ |
| | Segregation coefficient (k) | 0.1 |
| | Thermal expansion coefficient ($\beta$) | 2.5 $(10)^{-4}$ $K^{-1}$ |
| | **Associated dimensionless parameters** | |
| | Prandtl number $Pr = \nu/\kappa$ | 0.01 |
| | Peclet number $Pe = V_M L/\kappa$ | |
| | Schmidt number $Sc = \nu/D$ | 10 |
| | Density ratio $\sigma$ | 1.0 |
| | **Operating conditions** | |
| A] | Hot zone temperature ($T_H$) | 1331 K |
| | Distance between inlet and interface (L) | 1.0 cm |
| | Height of adiabatic zone | 2.5 mm |
| | Ampoule width (diameter) | 1.0 cm |
| B) | Hot zone temperature ($T_H$) | 1346 K |
| C) | Hot zone temperature ($T_H$) | 1251 K |
| D) | Ampoule width | 2.0 cm |
| E) | Ampoule width | 0.5 cm |
| V 1) | Translation (supply) rate ($V_m$) | 6.5 $\mu m\ s^{-1}$ |
| V 2) | Translation (supply) rate ($V_m$) | 3.25 $\mu m\ s^{-1}$ |
| V 3) | Translation (supply) rate ($V_m$) | 0.65 $\mu m\ s^{-1}$ |

Table 3. Compositional non-uniformity $\xi$ [%] for Ge:Ga

| | Residual Acceleration Magnitude [gal] | Orientation N | Orientation $e_g$ | Ampoule Width [cm] 1 | Growth Rate [$\mu m\ s^{-1}$] 6.5 | 1 3.25 | 1 0.65 | 0.5 6.5 | 2.0 6.5 |
|---|---|---|---|---|---|---|---|---|---|
| A) | $10^{-4}$ | ↑ | ← | | 80 | | | | |
| | $10^{-5}$ | | ← | | 92.7 | | 11.9 | 12.0 | |
| | | | ↙ | | 70.9 | | 11.3 | | |
| | | | ↓ | | 6.4 | | 0.95 | | |
| | $5(10)^{-6}$ | | ↓ | | 3.2 | | | | |
| | | | ↙ | | 39 | | | | |
| | | | ← | | 54.2 | | | | |
| | $10^{-6}$ | | ← | | 11.3 | | 2.0 | | |
| | | | ↙ | | 8.0 | | | | |
| B) | $10^{-4}$ | ↑ | ↓ | | 36 | | | | |
| | | | ↑ | | 32 | | | | |
| | $\sqrt{2}(10^{-5})$ | | ↙ | | 110 | | | | |
| | | | ← | | 152 (91) | | | | |
| | $10^{-5}$ | | ↓ | | 7.5 | 4.6 | 0.7 | | |
| | $5\sqrt{2}(10^{-6})$ | | ↙ | | 57 | | | | |
| | $\sqrt{2}(10^{-6})$ | | ↙ | | 10 | | | | |
| | | | ↑ | | 4.0 | | | | |
| | | | ↓ | | 2.0 | | | | |
| | | | ← | | 21.5 (26) | | 1.5 | | |
| | $10^{-6}$ | | ↓ | | 0.7 | 0.4 | 0.0 | | 3.8 |
| | $10^{-7}$ | | ↑ | | 1.0 | 0.5 | 0.2 | | |
| C) | $10^{-5}$ | ↑ | ← | | 22.6 | | | | 64.5 |
| | $10^{-6}$ | | ← | | 2.3 | | | | |

$e_g$ is the unit vector parallel to g, N is the normal vector to the crystal. L = 1 cm for all cases. Values in parentheses indicate 3-D results. A), B) and C) refer to the operating conditions listed in table 2.

Table 4. Summary of results for impulses

| Magnitude [gal] | Duration[s] | $\xi_{init}$ | $\xi_{max}$ | $\xi_{min}$ | $\tau_v$ [s] | $\tau_\xi$ [s] | $\tau_c$ [s] |
|---|---|---|---|---|---|---|---|
| $5\times10^{-3}$ (ap $10^{-6}$) | 1 | 11 | 40 | 0 | 3-400 | 260 | 2200 |
| $3\times10^{-3}$ (ap $\sqrt{2}\times10^{-6}$) | 1 | 22 | 26 | 0 | 3-400 | 260 | >2000 |
| $3\times10^{-3}$ (ap $\sqrt{2}\times10^{-6}$) | 0.1 | 22 | 22 | 17 | 50 | 350 | >1000 |
| $3\times10^{-3}$ (ap $\sqrt{2}\times10^{-6}$) | 1* | 22 | 76 | 17 | 3-450 | 225 | >2000 |
| $3\times10^{-3}$ (ap $\sqrt{2}\times10^{-6}$) | 1 | | | | | | |
| ($\sqrt{2}\times10^{-6}$) | no pulse | 22 | 76 | 17 | 3-450 | 225 | >2000 |
| $3\times10^{-3}$ (p $\sqrt{2}\times10^{-6}$) | 1 | | | | | | |

ap and p denote a pulse anti-parallel and parallel to the background acceleration. All pulses are parallel to the crystal-melt interface. The background accelerations are given in parentheses and the asterisk denotes a 1 second pulse that was was repeated once after a 1 second interval. The relaxation time $\tau_v$ refers to the decay time for the velocity field. $\tau_\xi$ denotes the time to reach the maximum value of $\xi$, and $\tau_c$ the time for the solute field to return to its initial steady state distribution.

**Fig. Captions**

Fig. 1. Idealized model of the Bridgman-Stockbarger system.

Fig. 2. The dimensionless temperature field, $\theta$, for 2-D calculations corresponding to operating conditions **B - V1** in table 2. Note that there is no difference between this and a purely conductive profile (i.e. g=0).

Fig. 3. a) The steady flow field produced by a residual acceleration with a magnitude $(10)^{-5}$ gal acting parallel to the crystal-melt interface. The maximum speeds are approximately twice the growth speed.

b) The dimensionless solute field, C, associated with the flow depicted in a). The contour interval is 0.9. For this case $\xi$= 92.7%.

Fig. 4. a) The steady flow field produced by a residual acceleration with a magnitude $5(10)^{-6}$ gal acting parallel to the crystal-melt interface. The maximum speeds are slightly greater than the growth speed.

b) The dimensionless solute field, C, associated with the flow depicted in a). The contour interval is 0.7. For this case $\xi$= 39%.

Fig. 5. a) The steady flow field produced by a residual acceleration with a magnitude $(10)^{-6}$ gal acting parallel to the crystal-melt interface. The maximum speeds are slightly greater than the growth speed.

b) The dimensionless solute field, C, associated with the flow depicted in a). For this case $\xi$= 11.3%.

Fig. 6. The steady flow field produced by a residual acceleration with a magnitude $(10)^{-5}$ gal acting perpendicular to the crystal-melt interface, otherwise the operating conditions are the same as for Figs. 3-5. The contour interval is 0.5. For this case $\xi$ = 6.4%.

Fig. 7. Lateral variations in melt composition at the interface for operating conditions corresponding to **A -V1** in table 2 with acceleration magnitudes of $10^{-5}$, $5x10^{-6}$ and $10^{-6}$ gal with a) parallel, b) 45° orientations c) perpendicular and with respect to the crystal-melt interface.

Fig. 8. Laterally averaged, axial composition profiles in the melt for operating conditions corresponding to **A - V1** in table 2 for accelerations with magnitudes of $10^{-5}$, $5x10^{-6}$ and $10^{-6}$ gal oriented a) parallel and b) perpendicular to the crystal-melt interface. Note that the latter are indistinguishable from the pure diffusion profile.

Fig. 9. a) The velocity field associated with a residual acceleration of magnitude $10^{-5}$ gal acting parallel to the crystal-melt interface. The operating conditions correspond to **A -V3** in table 2, i.e. the growth rate is 0.65 $\mu m\ s^{-1}$.

b) The dimensionless solute field associated with flow depicted in a). The contour interval is 0.2. For this case $\xi$= 11.9%.

Fig. 10. Lateral variations in melt composition at the interface in crystals grown from melts with different Schmidt numbers for accelerations with the following magnitudes and orientations with respect to the crystal-melt interface:
a) $10^{-5}$ gal parallel, b) $10^{-6}$ gal parallel and c) $10^{-5}$ gal perpendicular.

Fig. 11. Laterally averaged axial composition profiles for melts with different Schmidt numbers, for a $10^{-4}$ gal acceleration oriented parallel to the crystal-melt interface.

Fig. 12. The solute field at the crystal-melt interface consequent to a $\sqrt{2}(10)^{-5}$ gal acceleration oriented parallel to the interface for the 3-D case. The cross section is taken perpendicular to the ampoule axis. $\xi$ = 91%. The contour interval is 0.95

Fig. 13. The solute field at the crystal-melt interface consequent to $\sqrt{2}\ (10)^{-6}$ g acceleration oriented parallel to the interface for the 3-D case. The cross section is taken perpendicular to the ampoule axis . $\xi$ = 26%. The contour interval is 0.26.

Fig. 14. The solute field after the termination of a one second duration $0.5x10^{-2}$ gal impulse oriented parallel to the crystal-melt interface and anti-parallel to a steady $10^{-6}$ gal background: a) one second ($\xi$ = 11.3%), b) 30 seconds ($\xi$ = 0.67%), c) 250 seconds ($\xi$ = 40%) and d) 1250 seconds ($\xi$ = 3.4%).

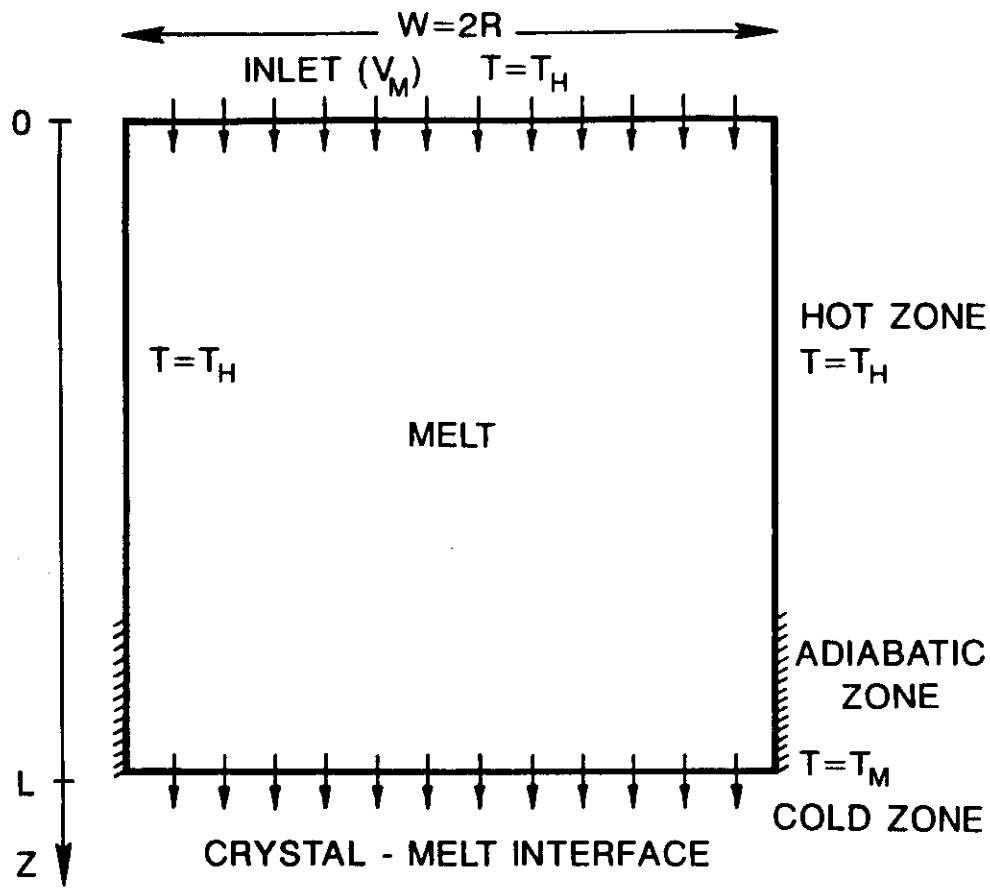
W=2R
INLET ($V_M$)
T=$T_H$
0
HOT ZONE
T=$T_H$
T=$T_H$
MELT
ADIABATIC
ZONE
T=$T_M$
L
COLD ZONE
Z
CRYSTAL - MELT INTERFACE

Fig.1

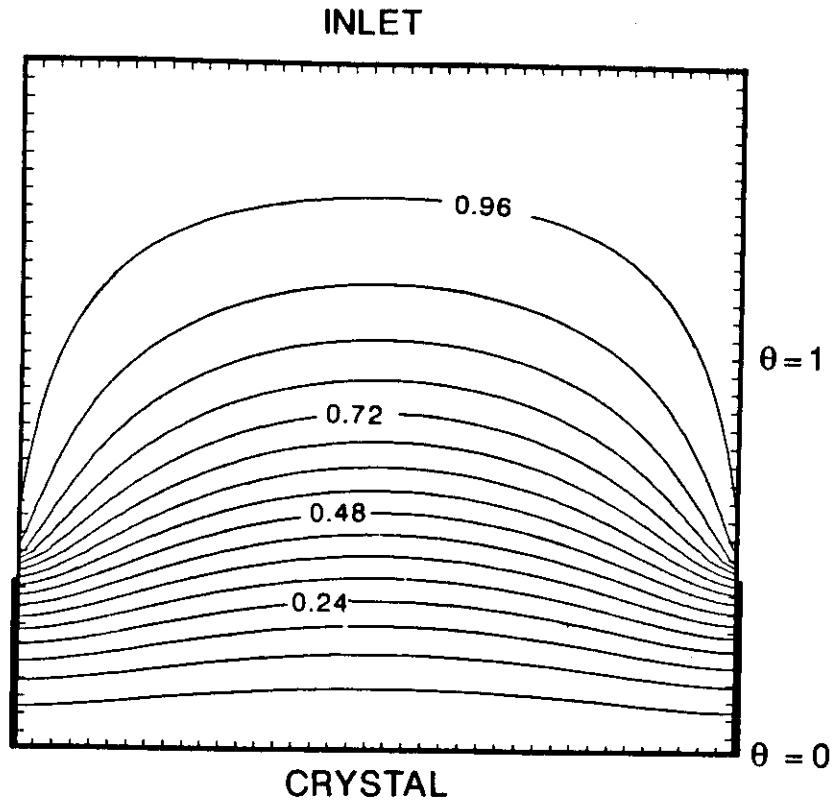
INLET
0.96
θ=1
0.72
0.48
0.24
θ=0
CRYSTAL

Fig.2

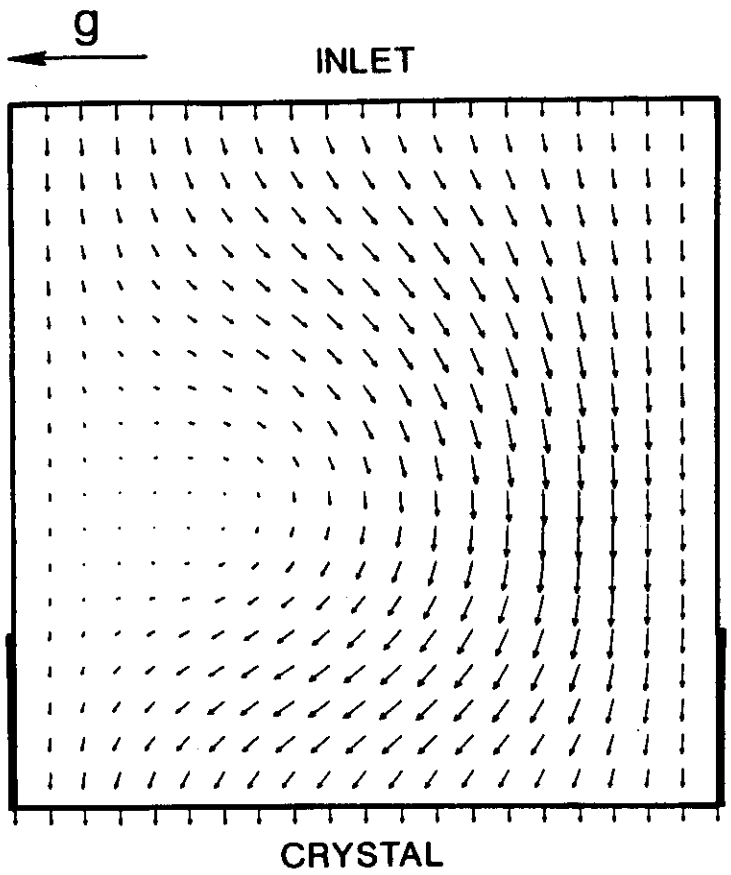


Fig.3a

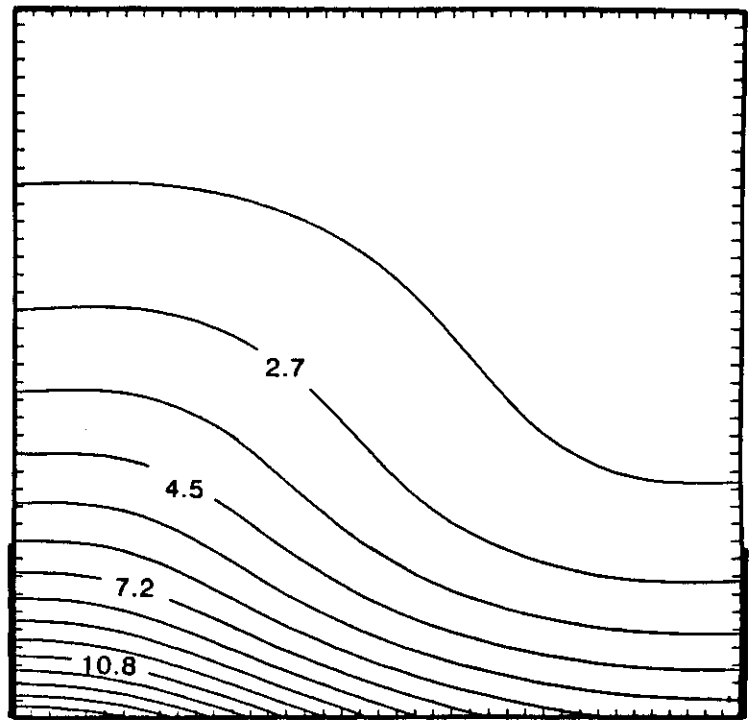


Fig.3b

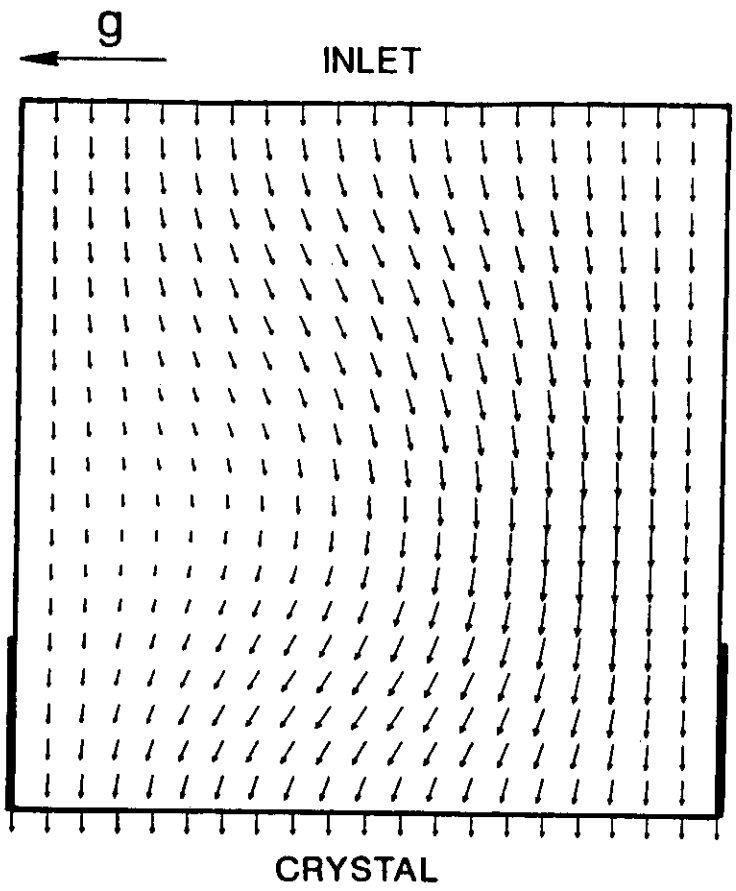


Fig.4a

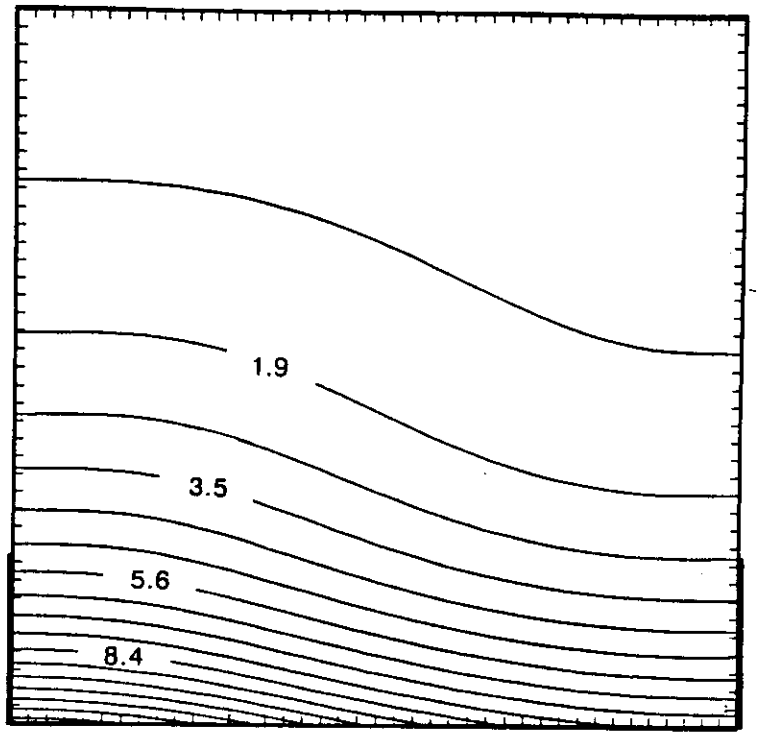


Fig.4b

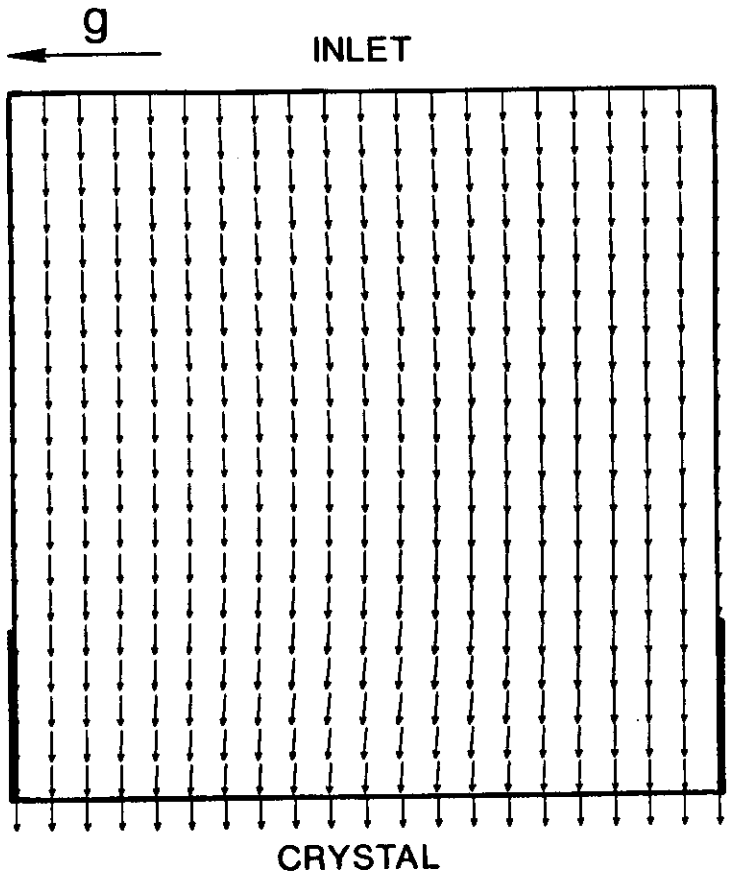


Fig.5a

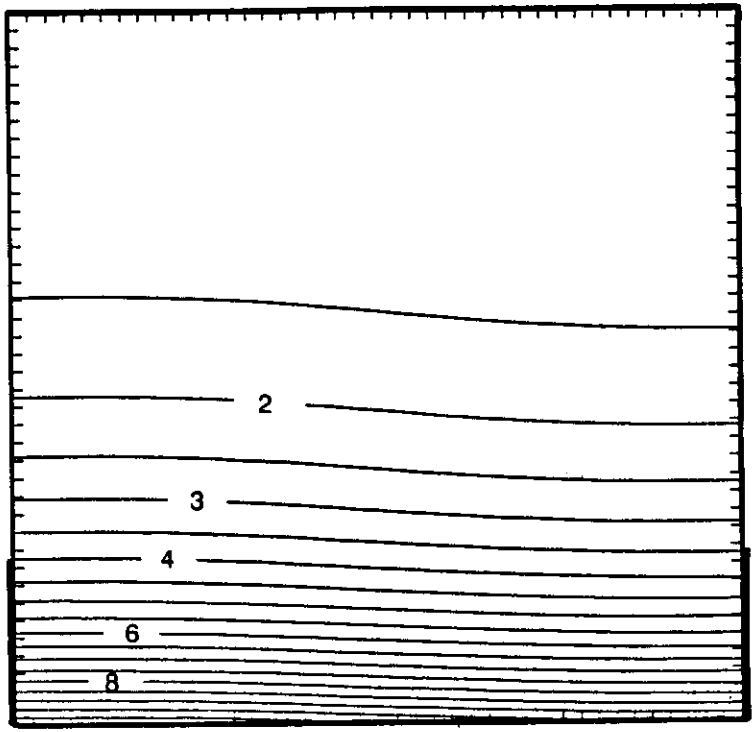


Fig.5b

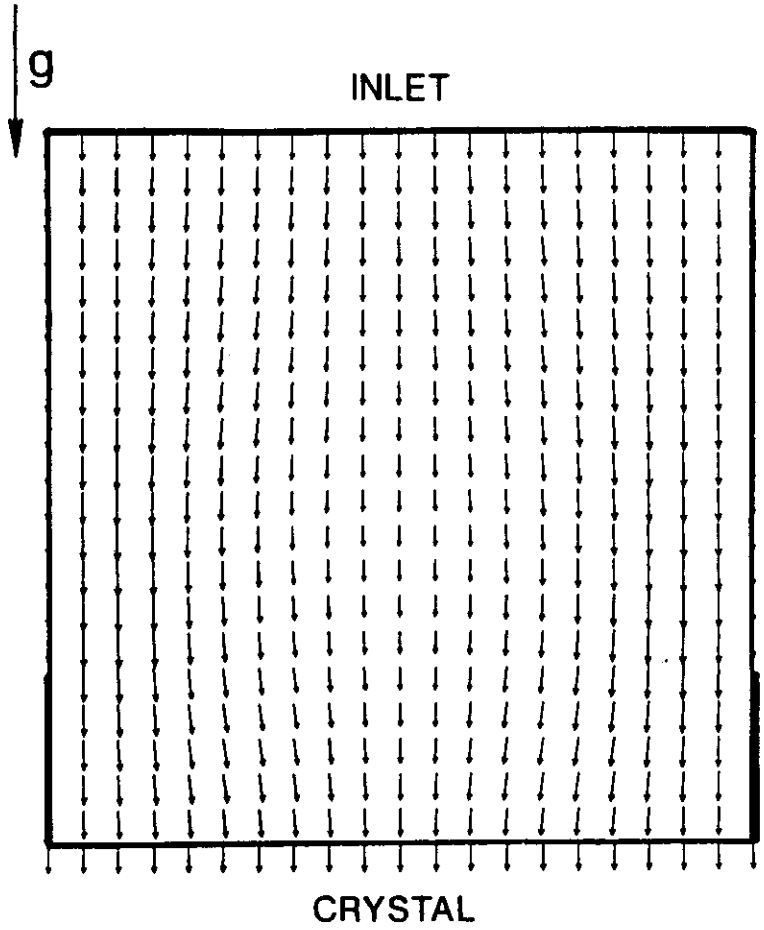
g
INLET
CRYSTAL

Fig.6

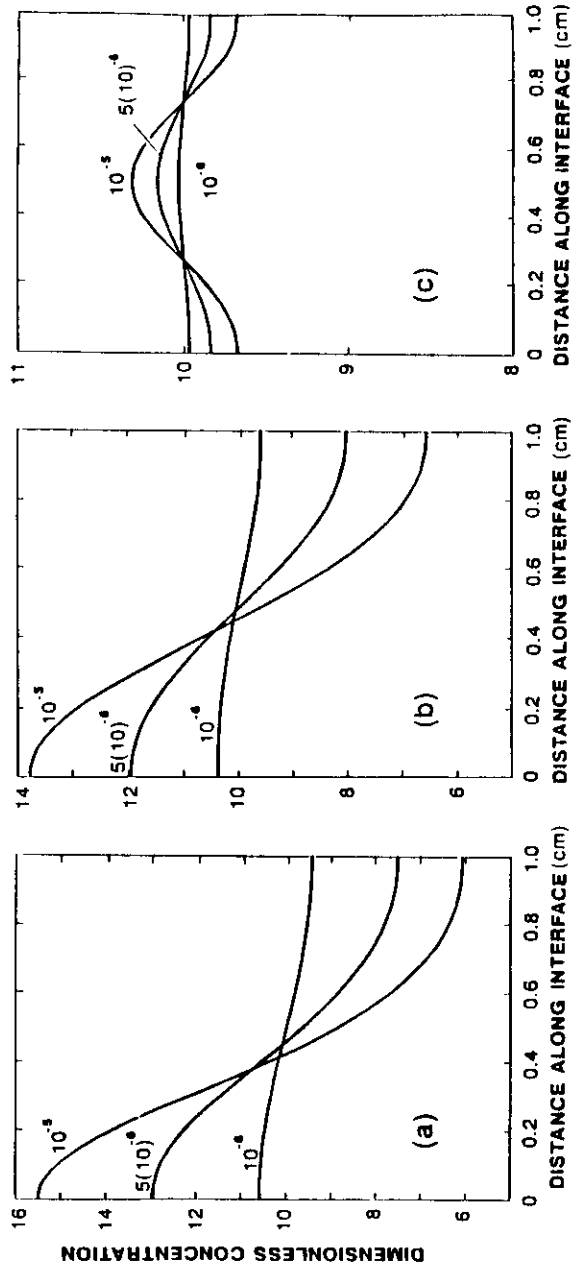
DIMENSIONLESS CONCENTRATION
DISTANCE ALONG INTERFACE (cm)
(a)
(b)
(c)
10^-5
5(10)^-6
10^-6

Fig.7

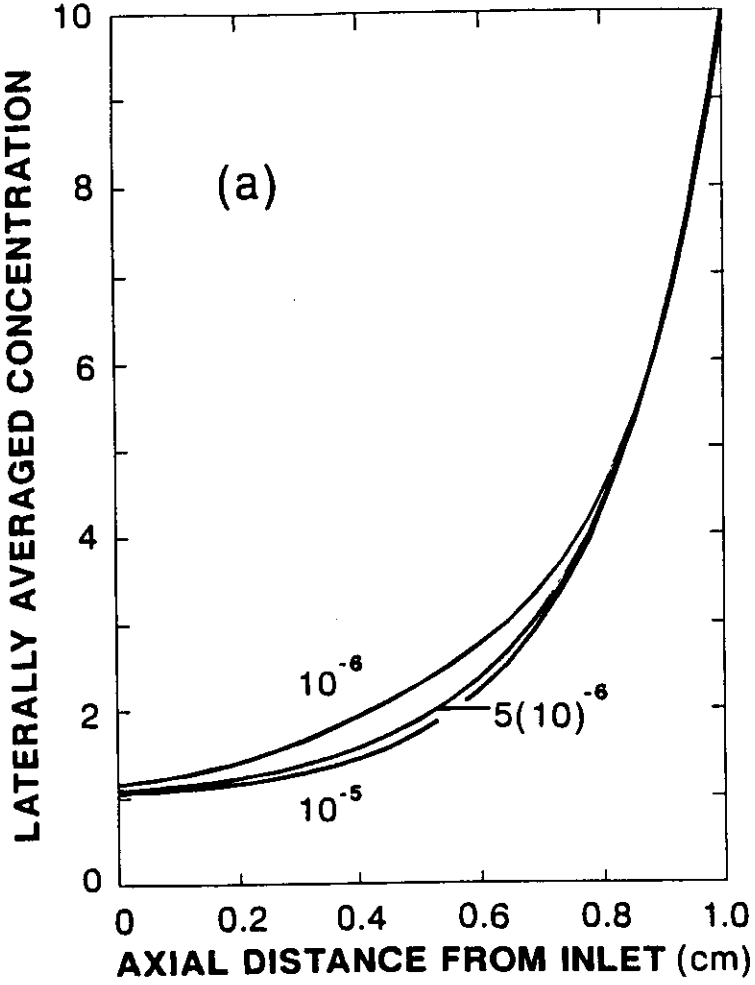
(a)
LATERALLY AVERAGED CONCENTRATION
AXIAL DISTANCE FROM INLET (cm)
10^-6
5(10)^-6
10^-5
0
2
4
6
8
10
0
0.2
0.4
0.6
0.8
1.0

Fig.8a

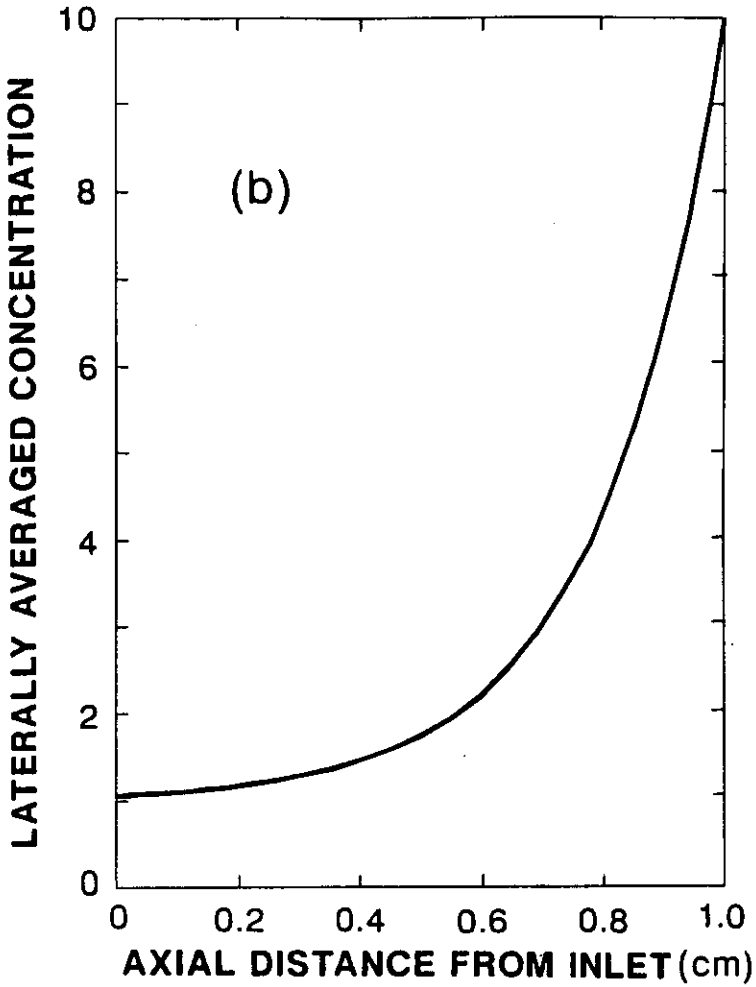
(b)
LATERALLY AVERAGED CONCENTRATION
AXIAL DISTANCE FROM INLET (cm)
0
2
4
6
8
10
0
0.2
0.4
0.6
0.8
1.0

Fig.8b

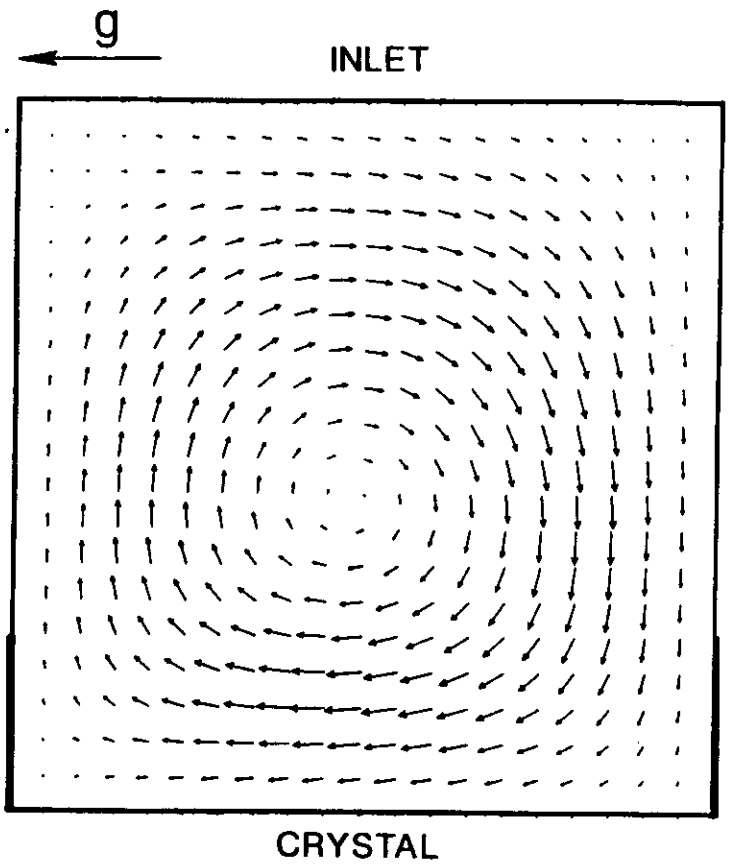


Fig.9a

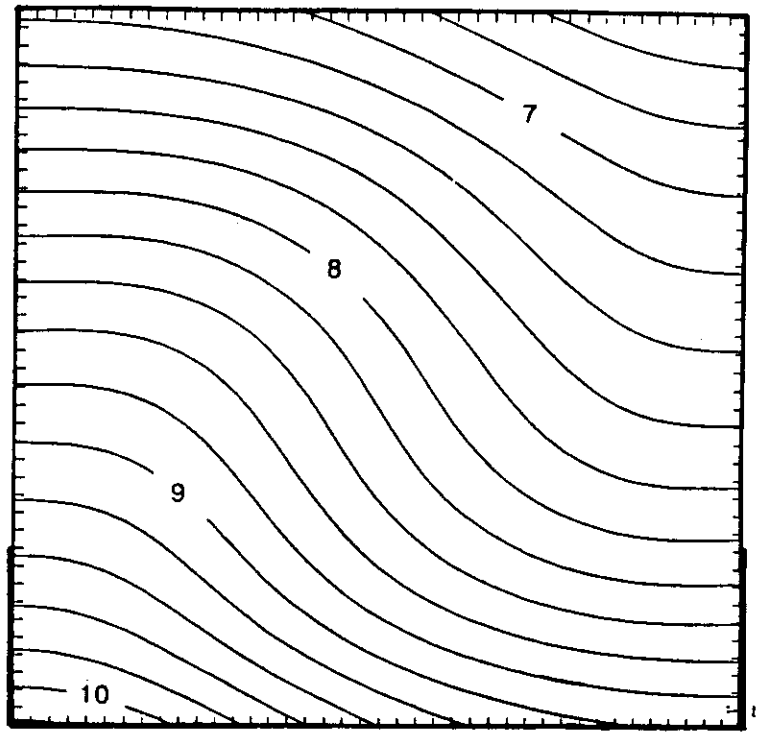


Fig.9b

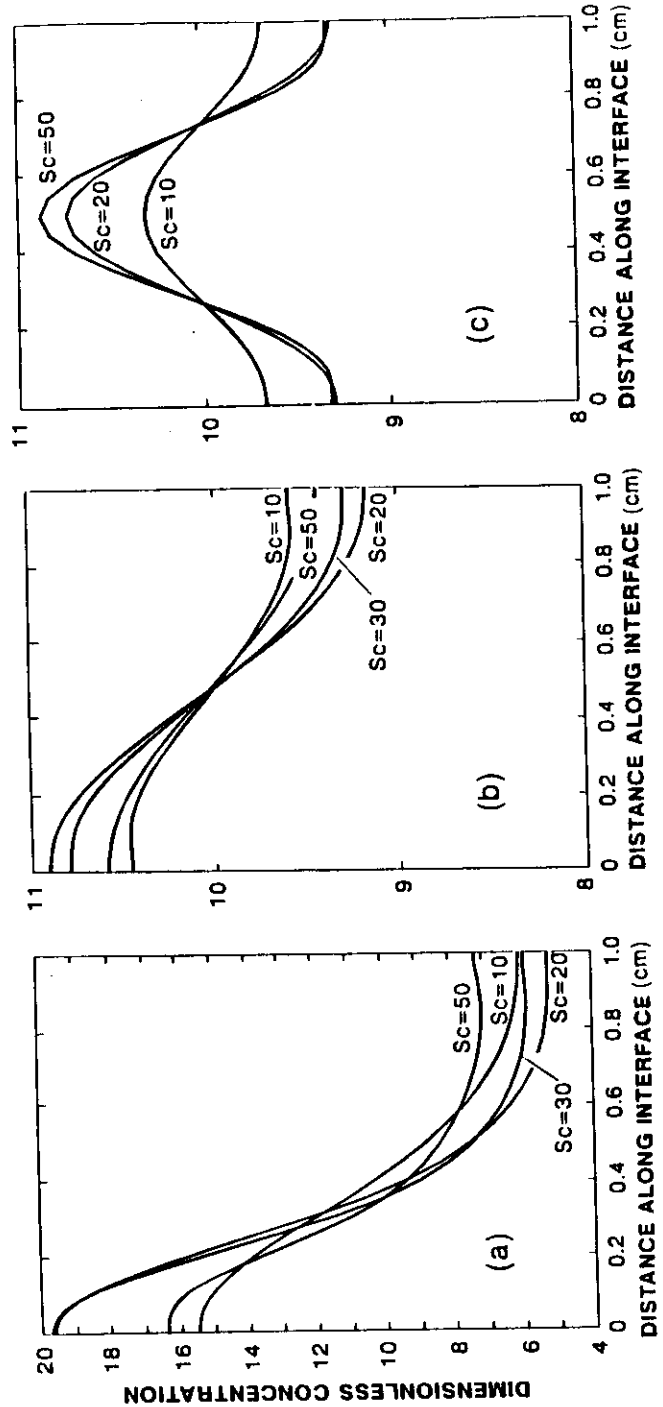
Sc=50
Sc=20
Sc=10
(c)
Sc=10
Sc=50
Sc=20
Sc=30
(b)
Sc=50
Sc=10
Sc=20
Sc=30
(a)
DIMENSIONLESS CONCENTRATION
DISTANCE ALONG INTERFACE (cm)

Fig.10

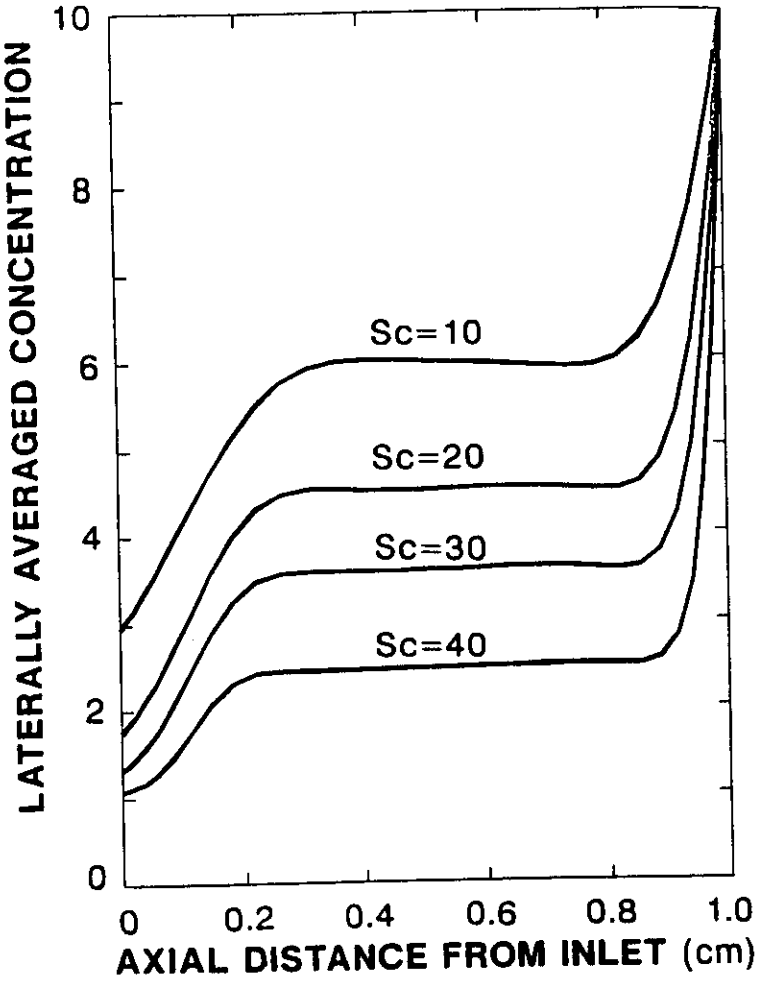
Sc=10
Sc=20
Sc=30
Sc=40
LATERALLY AVERAGED CONCENTRATION
AXIAL DISTANCE FROM INLET (cm)

Fig.11

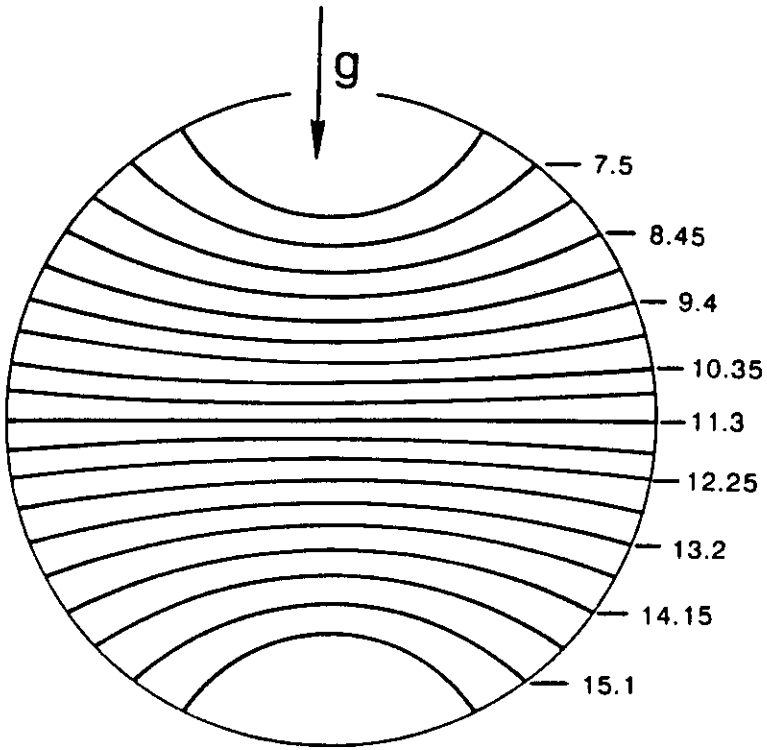
g
7.5
8.45
9.4
10.35
11.3
12.25
13.2
14.15
15.1

Fig. 12

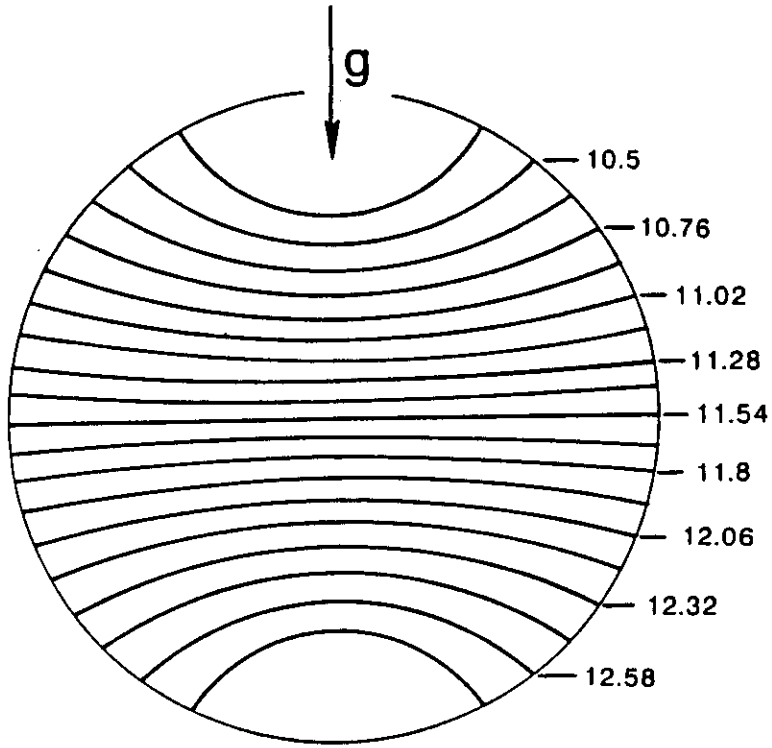
g
10.5
10.76
11.02
11.28
11.54
11.8
12.06
12.32
12.58

Fig. 13

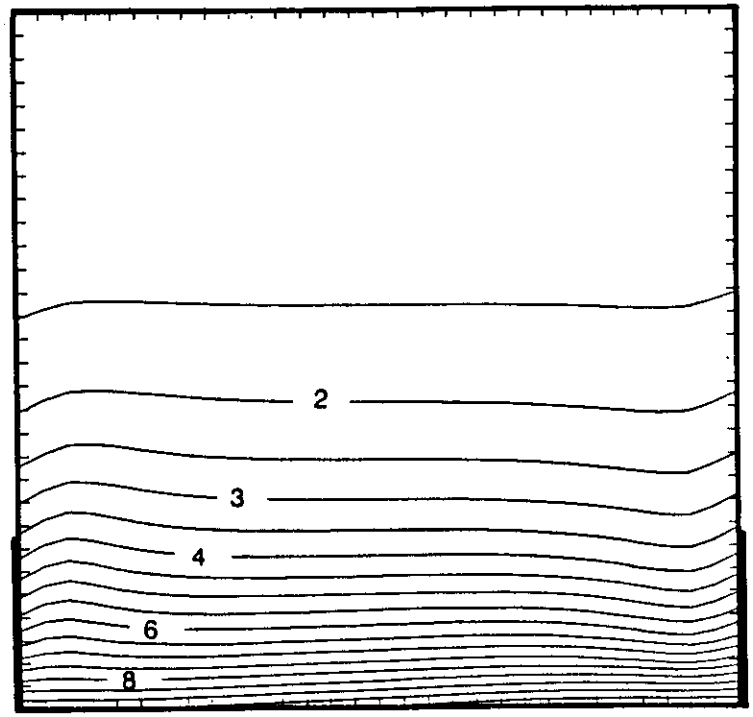


Fig.14a

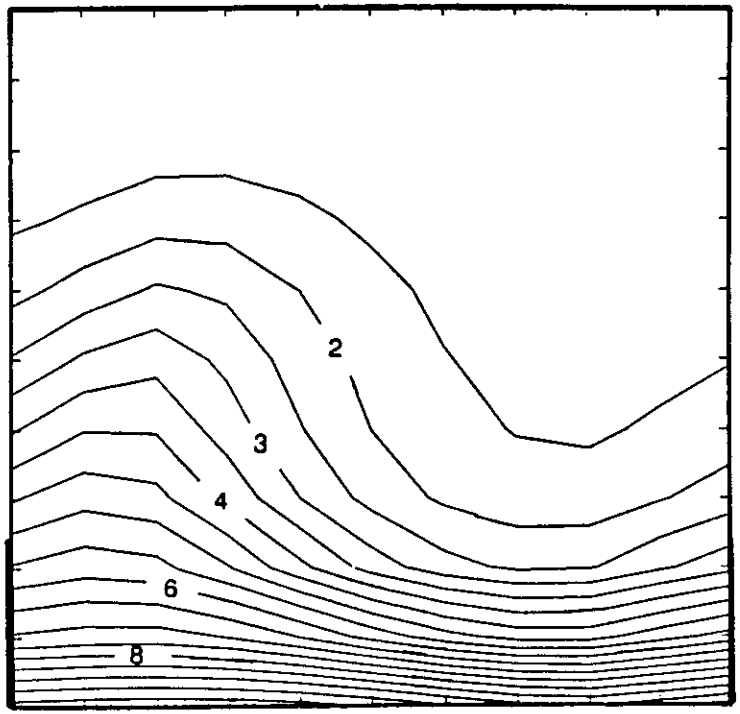


Fig.14b

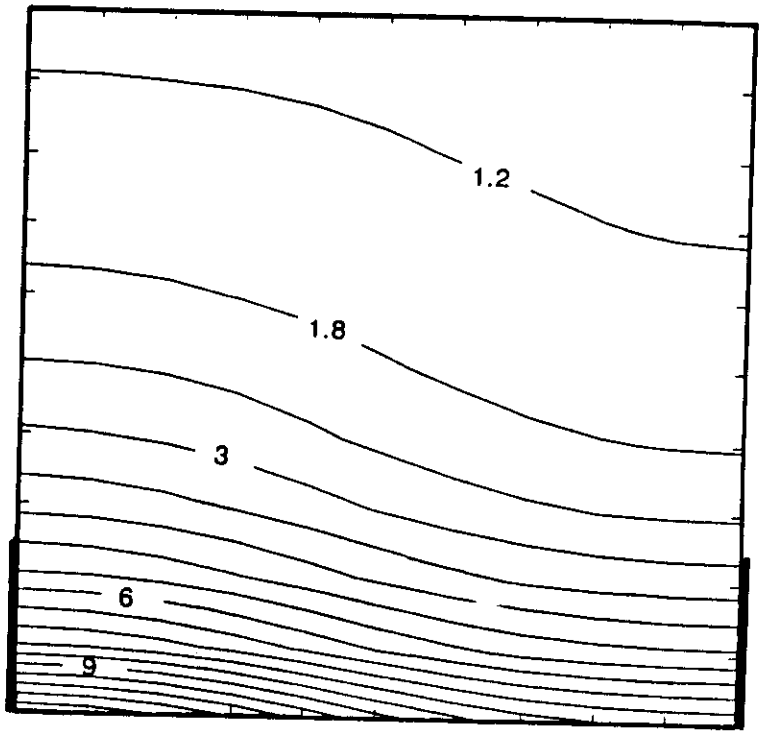


Fig.14c

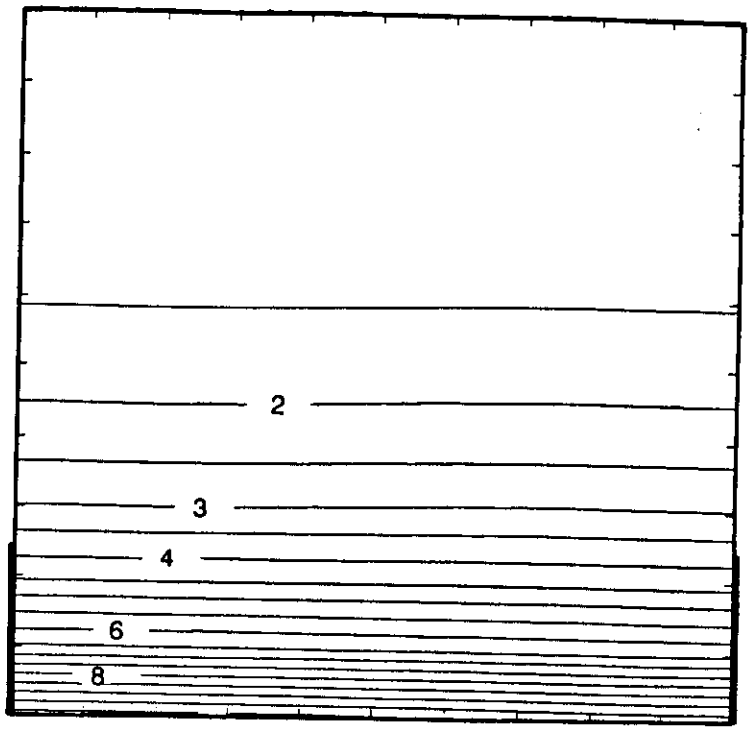


Fig.14d